2017 IEEE International Conference on Robotics and Automation (ICRA)
Singapore, May 29 - June 3, 2017

Development and Validation of Modeling Framework for Interconnected Tendon Networks in Robotic and Human Fingers

Taylor D. Niehues, Raymond J. King, Ashish D. Deshpande, Sean Keller

Abstract— **The primary contribution of this work is the development of a generalized modeling methodology for complex tendon systems toward a long-term goal of modeling the mechanical structure of the human finger. The key feature of this model is its ability to predict how muscle forces will transmit through an interconnected tendon network based on tendon kinematics and the current joint posture, so that the transformation from input muscle forces to output joint torques and fingertip forces is accurately represented. The feasibility of this model is evaluated by using a tendon-driven robotic finger testbed. Moreover, we utilize the validated model to explore unique features of the extensor mechanism.**

I. Introduction

The interconnected tendon structure of the human finger results in a complex relationship between the input muscle forces and the output joint torques and fingertip forces. The distribution of muscle tensions through the extensor mechanism, which is a network of interconnected tendons on the dorsal surface of human fingers (see Fig. 1), plays a critical role during everyday finger interactions and dynamic motions. A biomechanical model that fully captures the complex interactions within this interconnected tendon system would allow for an in-depth exploration of the unique features and functionality of the human finger.

In previous works of human finger modeling, tension distribution through the extensor mechanism has commonly been defined by constant ratios that split muscle forces between the various connecting tendons [2], [3]. A constant tension distribution may be valid in specific circumstances, i.e. static force production of a single muscle, but in reality the tension distribution ratios can vary significantly as a function of joint posture [4], relative activation levels of multiple muscles [5], and external forces/torques being applied to the finger.

T. D. Niehues and A. D. Deshpande are with the Department of Mechanical Engineering, University of Texas at Austin, Austin, Texas 78712, USA (email: taylor.niehues@utexas.edu, ashish@austin.utexas.edu)

R. J. King and S. Keller are with Oculus & Facebook, Redmond, WA 98052, USA (email: {raymond.king, sean.keller}@oculus.com)

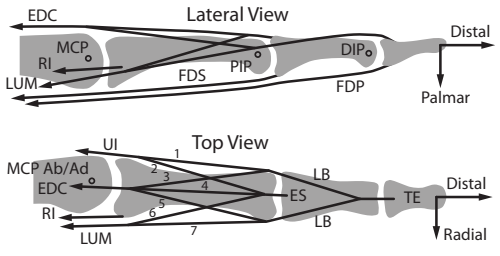

Fig. 1. Human finger schematic. The four finger degrees of freedom, metacarpophalangeal (MCP) abduction/adduction (ab/ad), MCP flexion/extension, proximal interphalangeal (PIP), and distal interphalangeal (DIP) joints, are actuated by six muscles: extensor digitorum communis (EDC), lumbrical (LUM), ulnar interosseous (UI), radial interosseous (RI), flexor digitorum profundus (FDP), and flexor digitorum superficialis (FDS). The extensor mechanism consists of seven connecting tendons that converge to two lateral bands (LBs), the extensor slip (ES), and the terminal extensor (TE). The RI inserts directly into the proximal phalange [1].

Research efforts have also been made to develop more advanced models that capture the kinematics of the human finger extensor mechanism and accurately predict how muscle forces distribute through the extensor mechanism in different scenarios. Kinematic models of the extensor mechanism have been developed with a strong focus on interphalangeal joint coupling [6], [7], but they have not been extended to model the transmission of muscle forces through the network. Other researchers have used optimization methods to determine tension distribution ratios within the extensor mechanism [8], [9]. While this provides a level of insight into the effects of tension distribution variations, it cannot be considered a working mechanical model. Recently, more complete and accurate models of interconnected tendon systems, such as the custom computational modeling environment of Valero-Cuevas et. al. [5] or bond graph tendon model of King [10], have been developed that are capable of capturing tension distribution as a function of system states, muscle inputs, and external interaction forces. These models require iterative numerical methods (i.e. relaxation algorithm [5] or forward simulation [10]) to determine the equilibrium state of the extensor mechanism, which restricts their application. Our goal in this work is to create a finger model that accurately captures extensor mechanism mechanics, is computationally efficient, and is versatile for multiple applications, e.g. for dynamic simulation, forward/inverse force prediction, or real-time implementation.

In this paper, we present and validate a generalized framework for modeling interconnected tendon systems. The functionality of the model is demonstrated by implementing a basic human finger model, and simulations demonstrate how dynamic variations in tension distribution are captured. Then, we test and validate the model using a tendon-driven robotic finger testbed with human-like tendon structure. We introduce a system identification method that utilizes observed interphalangeal joint coupling, which directly correlates to the structure and routing of the extensor mechanism, to improve model parameter estimation. Finally, we analyze the model's ability to accurately predict the force/torque transformations between the muscles, joints, and fingertip of the robotic finger.

II. Modeling of Interconnected Tendon Systems

In this section, we present a comprehensive framework for the mechanical modeling of complex interconnected tendon networks.

A. Force/Torque Relationships

One of the challenges when modeling complex tendon systems lies in identifying the effective moment arm matrix R that describes how muscle forces ($\mathbf{f}_m$) are converted into joint torques ($\boldsymbol{\tau}$). In general, the effective moment arms are considered a function of joint angles ($\boldsymbol{\theta}$), such that:

$$\boldsymbol{\tau} = R(\boldsymbol{\theta})\mathbf{f}_m \tag{1}$$

In addition to posture-dependent changes in tendon lines of action (e.g. tendon bow-stringing), joint angles also determine how muscle forces are distributed through the tendon network at any instant in time. Note that there may also exist load-dependent viscoelastic deformations, such that R is also a function of $\mathbf{f}_m$. The modeling framework presented here is capable of including load-dependent effects, but we have not included them in this work.

We begin by identifying moment arm functions for each tendon segment. We define $R_m(\boldsymbol{\theta})$ as a *direct* moment arm matrix containing instances where muscles directly cross the joints; in the human index finger, this matrix would contain all metacarpophalangeal (MCP) joint moment arms and all FDP and FDS moment arms (see Fig. 1). The connecting tendon moment arm matrix $R_{ct}(\boldsymbol{\theta})$ holds moment arm functions for all connecting tendon segments, e.g. the segments that make up the human finger extensor mechanism (segments numbered 1-7 in Fig. 1). Thus, the total torque being applied to the system is defined as

$$\boldsymbol{\tau} = R_m(\boldsymbol{\theta})\mathbf{f}_m + R_{ct}(\boldsymbol{\theta})\mathbf{f}_{ct} \tag{2}$$

Methods exist in the literature for identifying the moment arms $R_m(\boldsymbol{\theta})$ and $R_{ct}(\boldsymbol{\theta})$ in human fingers [1], [11], [12]. The only remaining unknown term is $\mathbf{f}_{ct}$, the tension in the connecting tendons. In the next section, we analyze the tendon kinematics to quantify how muscle forces transmit to connecting tendons depending on joint posture.

B. Tension Distribution

Here we describe a method for finding the tension distribution matrix $T(\boldsymbol{\theta})$ that quantifies how muscle forces transmit through junctions to the connecting tendons:

$$\mathbf{f}_{ct} = T(\boldsymbol{\theta})\mathbf{f}_m \tag{3}$$

The schematic in Fig. 2 shows a single muscle splitting into multiple connecting tendons.

We begin by describing the relative tendon length changes that occur as a function of joint angle. This can be found through integration of $R_{ct}(\boldsymbol{\theta})$:

$$\boldsymbol{\ell}_{ct}(\boldsymbol{\theta}) = \int R_{ct}^T(\boldsymbol{\theta})d\boldsymbol{\theta} + \boldsymbol{\ell}_{ct,init} \tag{4}$$

where $\boldsymbol{\ell}_{ct,init}$ describes the tendon resting lengths when all joint angles are zero.

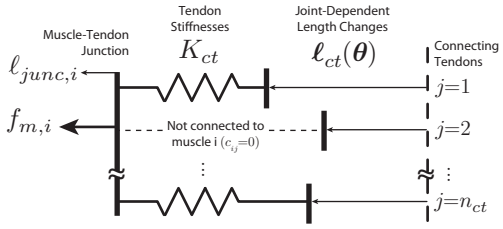

Fig. 2. Schematic of junction between muscle i and connecting tendons.

Next, given $\boldsymbol{\ell}_{ct}(\boldsymbol{\theta})$ and the muscle force $f_{m,i}$ applied by only muscle i, we find the resulting tensions $\mathbf{f}_{ct,i}$ in the connecting tendons. Connecting tendon stiffnesses are located in the diagonal matrix K_{ct}. In order to account for the fact that zero force can be transmitted to tendons that are not attached to muscle i, we define a constant tendon connection matrix C of the same size as $T(\boldsymbol{\theta})$, where $c_{ji} = 1$ if connecting tendon j is attached to muscle i and $c_{ji} = 0$ otherwise. Then, we can calculate the effective connecting stiffness matrix $K_{ct,i}$ for muscle i:

$$K_{ct,i} = \text{diag}(C_i)K_{ct} \tag{5}$$

where C_i is the i^{th} column of C. In this way, if tendon j is not attached to muscle i (e.g. tendon $j = 2$ in Fig. 2), element j of $K_{ct,i}$ is zero, so that no force from muscle i transfers to tendon j.

Then, the connecting tendon tensions that result from muscle force i can be found as:

$$\mathbf{f}_{ct,i} = K_{ct,i}\Big[\ell_{junc,i} - \boldsymbol{\ell}_{ct}(\boldsymbol{\theta})\Big]^+ \tag{6}$$

where $\ell_{junc,i}$ is the muscle junction position and $[\mathbf{x}]^+$ is an element-wise operator such that $x_k^+ = 0$ for $x_k \leq 0$ and $x_k^+ = x_k$ otherwise, which is required since tendons can only apply pulling forces. From static force analysis at the junction point, total muscle force $f_{m,i}$ is equal to the sum of connecting tendon tensions $\mathbf{f}_{ct,i}$:

$$f_{m,i} = \sum_{j=1}^{n_{ct}} f_{ct,ij} = \sum_{j=1}^{n_{ct}} k_{ct,i,j}\Big[\ell_{junc,i} - \ell_{ct,j}(\boldsymbol{\theta})\Big]^+ \tag{7}$$

Assuming knowledge of joint position $\boldsymbol{\theta}$ and applied muscle force $f_{m,i}$, we can solve Eq. (7) to find the junction position $\ell_{junc,i}$. Then, we can use Eq. (6) to calculate the connecting tendon forces $\mathbf{f}_{ct,i}$ that result from applied force f_{mi}, which we express as the function $\mathbf{f}_{ct,i}(\boldsymbol{\theta}, f_{m,i})$. Then, from Eq. (3), the i^{th} column of T is:

$$T_i(\boldsymbol{\theta}, f_{m,i}) = \frac{1}{f_{m,i}} \cdot \mathbf{f}_{ct,i}(\boldsymbol{\theta}, f_{m,i}) \tag{8}$$

An exception occurs when C_i is a zero vector; in this case, muscle i has no connections and T_i is simply a zero vector.

With Eq. (8), we have found how applied muscle forces will distribute through the connecting tendons as a function of $\boldsymbol{\theta}$ and $\mathbf{f}_m$. In order to produce a linear force-torque relationship as in Eq. (1), we can approximate Eq. (8) for a

constant operating muscle force f_{m0}, such that

$$T_i(\boldsymbol{\theta}) \approxeq \frac{1}{f_{m0}} \cdot \mathbf{f}_{ct,i}(\boldsymbol{\theta}, f_{m0}) \tag{9}$$

We will explore the effects of such an approximation in the next section.

Now, knowing $T(\boldsymbol{\theta})$ and combining Eqs. (1), (2), and (3), we can identify the effective moment arm matrix as:

$$R(\boldsymbol{\theta}) = R_m(\boldsymbol{\theta}) + R_{ct}(\boldsymbol{\theta})T(\boldsymbol{\theta}) \tag{10}$$

With this, we can find the joint torques $\boldsymbol{\tau}$ that will be produced for any joint configuration $\boldsymbol{\theta}$ and combination of muscle forces $\mathbf{f}_m$ using Eq. (1).

We can also define the change in muscle lengths $\boldsymbol{\ell}_m(\boldsymbol{\theta})$, without considering the effects of tendon compliance, as:

$$\boldsymbol{\ell}_m(\boldsymbol{\theta}) = \int R^T(\boldsymbol{\theta}) d\boldsymbol{\theta} \tag{11}$$

III. Case Study: Human Finger Model

In this section, we implement the presented framework to model the human finger (Fig. 1). We consider the finger to be a planar system for simplicity, and define the order of muscles and connecting tendons as in Fig. 1. The moment arm functions $R_m(\boldsymbol{\theta}) \in \mathbb{R}^{3\times 6}$ and $R_{ct}(\boldsymbol{\theta}) \in \mathbb{R}^{3\times 7}$ are equivalent to those proposed in [6]. The connection matrix $C \in \mathbb{R}^{7\times 6}$ is populated with ones at elements c_{13}, c_{23}, c_{31}, c_{41}, c_{51}, c_{62}, and c_{72}, and zeros elsewhere. We define $K_{ct} = \text{diag}\left([43, 75, 40, 126, 40, 75, 43]\right)\ \frac{N}{mm}$ based on human data from [13], choose a nominal operating force for all muscles of $f_{m0} = 10\ N$, and assume all connecting tendons are taut when joint angles are zero ($\boldsymbol{\ell}_{ct,init} = \mathbf{0}$).

A. Posture-Dependent Effective Moment Arms

The effective muscle moment arms of the muscles connected to the extensor mechanism (Fig. 3) show a sharp switching behavior as various connecting tendons become taut or slack. The curve along which a sharp moment arm change occurs represents the IP coupling curve (Fig. 3b). The effective PIP and DIP moment arms on each side of the coupling curve tend to stabilize the system toward the curve, producing the coordinated IP joint motions observed in human fingers [14]. The location and shape of the IP coupling curve depends on model parameters. Changes to connecting tendon rest lengths ($\boldsymbol{\ell}_{ct,init}$) act to translate the IP coupling curve up or down. Its slope and curvature are determined by the moment arm functions of the LB, ES, and TE tendons in $R_{ct}(\boldsymbol{\theta})$.

How sharply the effective moment arms switch depends upon the connecting tendon stiffnesses K_{ct} and the chosen operating force f_{m0}. The LUM and UI show less sharp moment arm changes than the EDC because of their relatively less stiff connecting tendons (Fig. 3d). A higher value of chosen operating muscle force f_{m0} also results in a less sharp change; conversely, as $f_{m0} \to 0$, moment arm switching becomes instantaneous. The approximation in Eq. (9) has the effect of setting a constant slope of moment arm switching, as opposed to a slope that varies dynamically as a function of muscle input force. In this work, the switching slope does not play a significant role, so the approximation is desirable for a linear force-torque relationship as in Eq. (1).

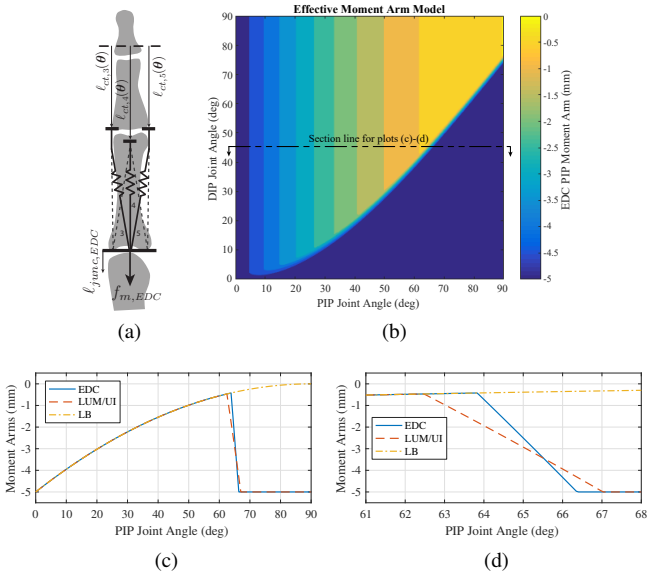

Fig. 3. Posture-dependent effective moment arms of extensor mechanism muscles. (a) Tendon schematic for the EDC muscle. The dashed lines in place of tendons 1, 2, 6, and 7 signify they do not attach to the EDC, i.e. $c_{j1} = 0$. The lengths of connecting tendons that do attach to the EDC can be found using Eq. (4). (b) Contour plot of the effective EDC moment arm across the PIP, as a function of PIP and DIP joint angle. In the top left section above the IP coupling curve, $\ell_{ct,3} \ll \ell_{ct,4}$, so all EDC force transmits through the LBs to the TE; in the bottom right section, $\ell_{ct,3} \gg \ell_{ct,4}$, so force transmits to the ES. (c) Section view of EDC, LUM, and UI moment arm functions for constant DIP angle $\theta_{DIP} = 45^o$. The EDC, LUM, and UI moment arms are equal to $r_{LB}(\boldsymbol{\theta})$ when LBs are taut (where r_{LB} is taken from [6]), then sharply shift down to $r_{ES} = -5$ mm as the tension shifts to the ES. (d) Enlarged view near the switching point.

B. Changing Tension Distribution

To demonstrate how muscle tensions dynamically distribute through the extensor mechanism, we performed a simulation study of a finger with a fingertip constraint that replicates a hard point contact (Fig. 4). Activation of any extensor mechanism muscles (i.e. EDC, LUM, or UI) tends to stabilize the PIP and DIP angles toward the IP coupling curve. Then, when a disturbance is introduced, in this case through activation of the FDP or FDS, small joint angle changes dynamically alter the tension distribution to connecting tendons (Fig. 4c) until the system re-stabilizes to a new equilibrium state. These tension distribution variations change the effective moment arms of extensor mechanism muscles, and thus also change their contribution to force production at the fingertip (Fig. 4d).

IV. Experimental Results

The proposed tendon model is tested and validated using a robotic finger with customizable tendon routing (Fig. 5). In this section, we will first describe how the model parameters are identified for the robotic finger with human-like tendon structure. Then, we demonstrate the capabilities of the interconnected tendon model in capturing complex muscle-to-fingertip force transformations.

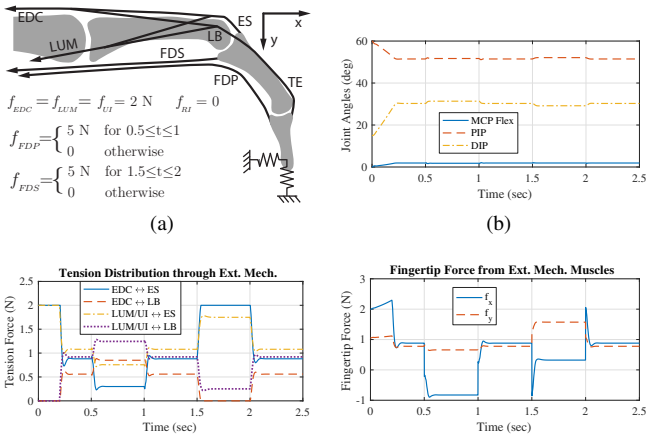

Fig. 4. Simulation of a human finger model. Because dynamic response is not critical for our analysis, finger inertia and damping are chosen heuristically to produce a fast, damped response. (a) Simulation conditions and input muscle forces. Fingertip translational position is stiffly constrained, while fingertip angle is allowed to rotate freely, replicating a hard point contact with no slipping. (b) Simulated joint angles. Tensions in the muscles of the extensor mechanism act to stabilize the finger in a coupled pose. (c) Force distribution to connecting tendons ($\mathbf{f}_{ct}$), which change in response to disturbance forces such as the activation of the FDP or FDS. (d) Fingertip force contribution from only the extensor mechanism muscles (EDC, LUM, and UI). Changes in tension distribution alter the resultant fingertip force produced by these muscles, despite constant input muscle tensions and minimal changes in joint angle.

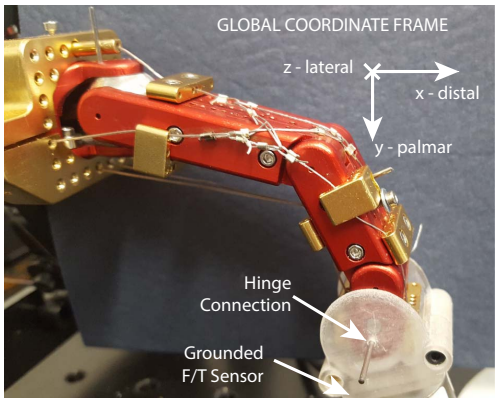

Fig. 5. Robotic finger testbed with customizable tendon routing, originally designed and manufactured by Si Tech Engineering (Snoqualmie, WA). Tendons are connected to force-controllable moving coil linear actuators (LCA50-050-75-2, SMAC Corporation, Carlsbad, CA) with in-line tension load cells (MLP-10, Transducer Techniques, LLC, Temecula, CA). Finger joints contain embedded angle sensors (AS5048 Magnetic Rotary Encoder, ams AG, Premstaetten, Austria). For fingertip force analysis, a grounded six-axis force/torque transducer (F/T Nano17 SI-50-0.5, ATI Industrial Automation, Garner, NC) is connected to the fingertip using an adapter that constrains fingertip position but allows free rotation of the distal link.

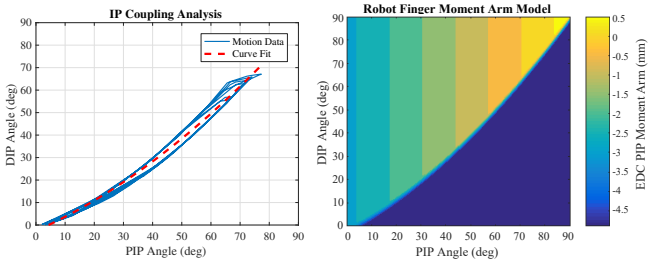

Fig. 6. Model parameter identification to correctly replicate observed IP coupling. (a) With the extensor mechanism muscles (EDC and LUM) taut, FDP contraction/extension results in PIP/DIP joint motions along the coupling curve. (b) To replicate the observed IP coupling in the model, we enforce a constraint that the LB and ES are both taut along this curve, or $\ell_{LB}(\boldsymbol{\theta}) = \ell_{ES}(\boldsymbol{\theta})$. The DIP moment arm of the TE and PIP moment arm of the ES are assumed to be constant, while the PIP moment arm of the LB is modeled as a first-order function of PIP angle.

A. Experimental Setup

In this work, the tendon routing and interconnections of the robotic finger were designed to mimic human finger structure. We implemented the two flexors (FDP and FDS), extensor (EDC), and LUM muscles. In order to provide insights that are significant for our complex tendon model, we do not focus on lateral fingertip forces that depend only upon MCP ab/ad moment arms. The interosseous muscles are not included because the UI has a virtually identical function as the LUM in the lateral x-y plane and the RI acts only on the MCP joint. For fingertip force analysis, we constrain fingertip position but allow free rotation of the distal link, simulating a hard point contact at the fingertip

B. Model Parameter Identification

To identify tendon moment arms, we collect extensive tendon kinematic data by measuring tendon excursions as the joints are moved through their range of motion. Then, moment arms can be determined by finding the gradient of a forward kinematic mapping [1], [12]. The direct moment arm functions $R_m(\boldsymbol{\theta})$ were estimated by fitting a second-order forward kinematics function, i.e. $\hat{\boldsymbol{\ell}}_m(\boldsymbol{\theta}) = \frac{1}{2}A\left(\boldsymbol{\theta}^2\right) + B\boldsymbol{\theta} + \mathbf{c}$, using a least-square regression of tendon kinematic data. Through differentiation $r_{ij}(\boldsymbol{\theta}) = \frac{\partial \hat{\ell}_{m,j}}{\partial \theta_i} = a_{ji}\theta_i + b_{ji}$, we find first-order moment arm functions to populate $R_m(\boldsymbol{\theta})$, which are considered sufficient to capture the angle-dependent moment arm variations in our system. Where muscles do not directly cross the joints, the corresponding elements of R_m are set to zero.

Next, in order to identify the moment arm parameters R_{ct} and resting lengths $\boldsymbol{\ell}_{ct,init}$ of connecting tendons, we combine tendon kinematic data with additional motion data to identify finger joint coupling. We set up a nonlinear optimization problem to minimize error between the predicted excursions $\boldsymbol{\ell}_m(\boldsymbol{\theta})$ from Eq. (11) and tendon excursion measurements while simultaneously enforcing the constraint to reproduce observed IP coupling (see Fig. 6 for details). Including IP coupling data in the parameter identification process reduces the parameter solution space, leading to more robust and accurate parameter estimation. The optimized model results in a muscle excursion RMS error of 1.54 mm for a kinematic data set of 700 points.

C. Forward Problem: Fingertip Force Prediction

Here we examine the accuracy of prediction of the fingertip force vector that is produced by a given combination of applied muscle forces. Joint angle measurements $\boldsymbol{\theta}$ are

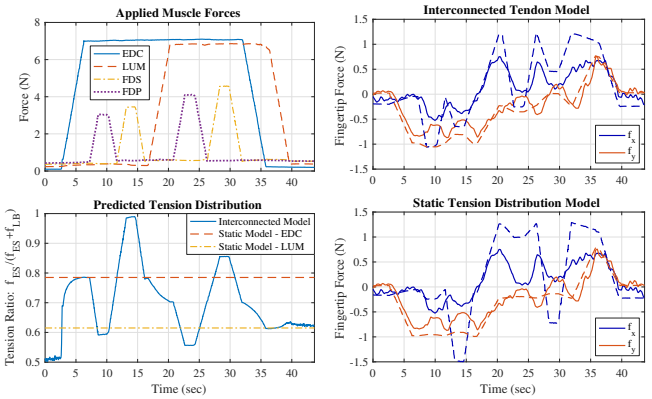

(a) (b)

Fig. 7. Experimental results for forward model predictions. (a) Chosen muscle force pattern (top) and predicted tension distribution ratio (bottom) represented as the fraction of EDC and LUM forces that transmit to the ES tendon. The values for the static tension distribution model, chosen to reproduce single-muscle force production of the EDC and LUM, are included for comparison. (b) Resultant fingertip forces in the lateral plane. Actual values are from the fingertip F/T sensor. The top plot shows fingertip force predictions based on the interconnected tendon model with muscle forces as input (RMSE = 0.29 N), while the bottom plot shows predictions based on a static tension distribution model (RMSE = 0.43 N). The static model also results in a significant fingertip torque, such that a forward simulation of fingertip point contact would predict unrealistic DIP hyper-extension or hyper-flexion.

used to calculate the Jacobian matrix that transforms fingertip forces $\mathbf{f}_x = [f_x, f_y, f_z, \tau_{dist}]^T$, where τ_{dist} is an external torque applied to the distal phalange, into joint torques:

$$\boldsymbol{\tau} = J^T(\boldsymbol{\theta})\mathbf{f}_x \tag{12}$$

As long as the finger is not in a singularity position, the Jacobian is a full-rank matrix, meaning we can also calculate the inverse relation $\mathbf{f}_x = J^{-T}(\boldsymbol{\theta})\boldsymbol{\tau}$.

Because the joint-dependent effective moment arm functions change abruptly near the IP coupling curve, it is infeasible to use joint angle measurements to directly determine $R(\boldsymbol{\theta})$. In our setup or during any hard point contact, the distal link of the finger can freely rotate about that contact point, such that $\tau_{dist} \approx 0$. One possible method is to input measured muscle forces into a forward simulation to find where the system stabilizes, which would provide the tension distribution and effective moment arms $R(\boldsymbol{\theta})$ as functions of time. However, the system ordinary differential equations (ODEs) become very stiff near the IP coupling curve, which causes numerical ODE solutions to become computationally inefficient and unreliable. An alternative method that we use here is to directly identify the tension distribution ratios using an optimization that minimizes $|\tau_{dist}|$ for a given set of muscle forces.

Experimental results in Fig. 7 demonstrate the model's forward prediction capabilities for chosen combinations of muscle forces. We verified that our optimization method produces identical results when compared to forward simulation after settling of transient effects, but optimization is computationally much more efficient. The tendon structure is designed with similar tendon stiffnesses and tension

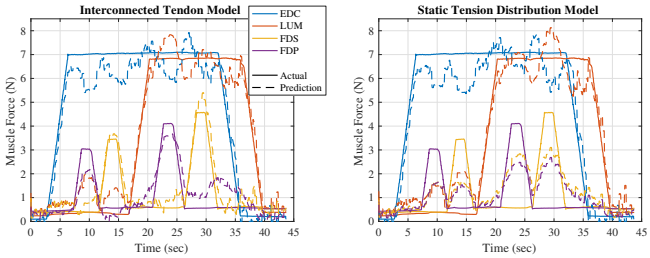

(a) (b)

Fig. 8. Inverse prediction of muscle forces based on measured fingertip forces. (a) Muscle force prediction using interconnected tendon model (RMSE = 0.61 N). (b) Prediction using static tension distribution model (RMSE = 0.91 N). In both cases, actual muscle force values are utilized in the optimization algorithm in Eq. (13) as muscle force estimates $\mathbf{f}_{m,est}$.

switching curves for the EDC and LUM, such that the tension distribution ratios are approximately equivalent in all postures. Thus, we assume one parameter $\alpha \in [0, 1]$ is required, where α of the EDC and LUM tensions transmit to the ES and the other $(1 - \alpha)$ transmit to the TE.

The interconnected tendon model provides a relatively accurate prediction of fingertip force (Fig. 7b, top). We suspected that the errors were caused by unmodeled frictional effects at tendon routing points. In a separate test, we held the EDC and LUM taut at $5\ N$, then slightly disturbed the finger in multiple directions and let it return to its original pose. We observed a fingertip force hysteresis of up to $\pm 0.5\ N$ oriented primarily in the x-direction. This corresponds well to the observed prediction errors, supporting the claim that friction is the cause of model prediction errors.

Without the ability to capture changes in tension distribution through the extensor mechanism, a static model fails to accurately predict the fingertip forces produced when multiple muscles are activated. To demonstrate this, we also present results using a model with static tension distribution ratios (Fig. 7b, bottom). Distribution values were chosen such that when the EDC or LUM are activated individually (e.g. at $t \approx 6$ and $t \approx 36$ seconds), fingertip force prediction matches measured results; however, as multiple muscles become active, forward prediction using the static model cannot replicate experimental data.

D. Inverse Problem: Muscle Force Prediction

The inverse problem predicts muscle forces given externally applied forces/torques. This represents an underdetermined problem, so optimization is helpful to choose an appropriate solution depending on a chosen cost function. We generalize the optimization problem as follows:

$$\begin{aligned} \underset{\hat{\mathbf{f}}_m, \boldsymbol{\alpha}}{\text{minimize}} \quad & \sum_{i=1}^{n_m} \left[\hat{f}_{mi} - f_{mi,est} \right]^2 \\ \text{subject to} \quad & \mathbf{f}_x = J^{-T}(\boldsymbol{\theta}) R(\boldsymbol{\theta}, \boldsymbol{\alpha}) \hat{\mathbf{f}}_m \\ & \hat{f}_{mi} \geq 0\ ,\ \alpha_j \in [0, 1] \end{aligned} \tag{13}$$

where $\hat{\mathbf{f}}_m$ are predicted muscle forces and $\boldsymbol{\alpha}$ contains the necessary tension distribution ratios to populate the T matrix

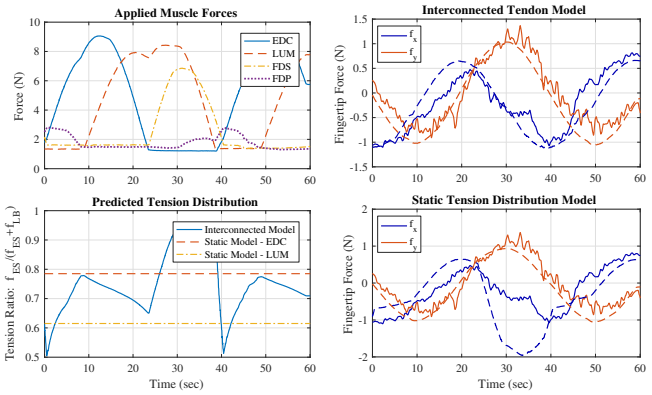

(a) (b)

Fig. 9. Experimental results for Cartesian fingertip force control for a circular commanded force trajectory in the x-y plane of radius 1 N. (a) Measured muscle tensions and tension distribution ratios for each model. (b) Measured fingertip force and predictions for the interconnected model (top, RMSE = 0.27 N) and the static tension distribution model for comparison (bottom, RMSE = 0.57 N). Predicted forces are calculated using muscle force measurements from tendon load cells, and differ slightly from original controller force commands due to actuator nonlinearities, creating slight deformations from the desired unit circle.

(i.e. T is a function of $\boldsymbol{\alpha}$ instead of $\boldsymbol{\theta}$). By defining $\boldsymbol{\alpha}$ explicitly, we avoid including $\boldsymbol{\theta}$ as an optimization variable, which could lead to unexpected results due to the angle-dependent nature of J, R_m, and R_{ct}. As in the previous case, only one α parameter is required corresponding to both EDC and LUM tension distribution. Because we have not included UI or RI muscles in our setup, the row corresponding to lateral force f_z is omitted from the equality constraint.

Muscle force predictions with the interconnected model are significantly more accurate than a static distribution model (Fig. 8), even though we provided precise muscle force estimates $\mathbf{f}_{m,est}$ from tendon load cells in both cases. Both models are constrained to produce zero fingertip torque τ_{dist}, corresponding to a hard point contact. In the static model, this constraint forces the FDP and FDS activations to remain somewhat coordinated, such that their fingertip torque contributions offset. In the interconnected model, the FDP and FDS muscles can be independently activated while maintaining zero net fingertip torque because the extensor mechanism naturally offsets the resulting τ_{dist} to hold the finger's coupled pose.

E. Cartesian Force Control using Complex Tendon Model

Next, we demonstrate the feasibility of implementing the model for active control of Cartesian fingertip force using the tendon actuators. The controller performs the optimization in Eq. (13) with $\mathbf{f}_{m,est} = 0$ to find the least-norm solution of muscle forces. We commanded a circular fingertip force profile in the lateral plane, with zero fingertip torque and no constraint on lateral force production (see Fig. 9).

V. Conclusions

We've presented a modeling framework for complex interconnected tendon systems, and demonstrated its capabilities using a tendon-driven robotic finger testbed. Fingertip force prediction was shown to be more accurate than a standard static tension distribution model, demonstrating the benefit of accurately replicating muscle force transmission through the extensor mechanism. We also illustrated the model's ability to solve the inverse problem, in which muscle forces are estimated based on observed external forces/torques and, if available, rough muscle force estimates (e.g. EMG measurements). We further demonstrated the versatility of the model by implementing it directly in a fingertip Cartesian force control algorithm. The presented results are limited to a simplified human-like tendon structure and rigid routing points, but this work represents an improvement toward an anatomically accurate human finger model and a better understanding of the human hand's unique functionality.

References

[1] K. An, Y. Ueba, E. Chao, W. Cooney, and R. Linscheid, "Tendon excursion and moment arm of index finger muscles," *Journal of Biomechanics*, vol. 16, no. 6, pp. 419–425, 1983.

[2] E. Chao and K.-N. An, "Graphical interpretation of the solution to the redundant problem in biomechanics," *Journal of Biomechanical Engineering*, vol. 100, no. 3, pp. 159–167, 1978.

[3] F. J. Valero-Cuevas, F. E. Zajac, and C. G. Burgar, "Large index-fingertip forces are produced by subject-independent patterns of muscle excitation," *Journal of Biomechanics*, vol. 31, no. 8, pp. 693–703, 1998.

[4] S. W. Lee, H. Chen, J. D. Towles, and D. G. Kamper, "Effect of finger posture on the tendon force distribution within the finger extensor mechanism," *Journal of Biomechanical Engineering*, vol. 130, no. 5, p. 051014, 2008.

[5] F. J. Valero-Cuevas, J.-W. Yi, D. Brown, R. V. McNamara, C. Paul, and H. Lipson, "The tendon network of the fingers performs anatomical computation at a macroscopic scale," *IEEE Transactions on Biomedical Engineering*, vol. 54, no. 6, pp. 1161–1166, 2007.

[6] J. N. A. L. Leijnse and J. J. Kalker, "A two-dimensional kinematic model of the lumbrical in the human finger," *Journal of Biomechanics*, vol. 28, no. 3, pp. 237–249, Mar. 1995.

[7] J. Leijnse, P. Quesada, and C. Spoor, "Kinematic evaluation of the fingers interphalangeal joints coupling mechanism – variability, flexion-extension differences, triggers, locking swanneck deformities, anthropometric correlations," *Journal of Biomechanics*, vol. 43, no. 12, pp. 2381–2393, 2010.

[8] H. J. Buchner, M. J. Hines, and H. Hemami, "A dynamic model for finger interphalangeal coordination," *Journal of Biomechanics*, vol. 21, no. 6, pp. 459–468, 1988.

[9] N. Brook, J. Mizrahi, M. Shoham, and J. Dayan, "A biomechanical model of index finger dynamics," *Medical Engineering & Physics*, vol. 17, no. 1, pp. 54–63, Jan. 1995.

[10] R. J. King, "Development and validation of a bond graph tendon model of the human finger with the Anatomically Correct Testbed (ACT) hand," Ph.D. dissertation, The University of Utah, 2015.

[11] N. Fowler, A. Nicol, B. Condon, and D. Hadley, "Method of determination of three dimensional index finger moment arms and tendon lines of action using high resolution MRI scans," *Journal of Biomechanics*, vol. 34, no. 6, pp. 791–797, Jun. 2001.

[12] A. Deshpande, R. Balasubramanian, J. Ko, and Y. Matsuoka, "Acquiring variable moment arms for index finger using a robotic testbed," *IEEE Transactions on Biomedical Engineering*, vol. 57, no. 8, pp. 2034–2044, 2010.

[13] M. Garcia-Elias, K.-N. An, L. J. Berglund, R. L. Linscheid, W. P. Cooney, and E. Y. Chao, "Extensor mechanism of the fingers. II. Tensile properties of components," *The Journal of Hand Surgery*, vol. 16, no. 6, pp. 1136–1140, 1991.

[14] J. Leijnse, J. Bonte, J. Landsmeer, J. Kalker, J. Van der Meulen, and C. Snijders, "Biomechanics of the finger with anatomical restrictions – the significance for the exercising hand of the musician," *Journal of Biomechanics*, vol. 25, no. 11, pp. 1253–1264, 1992.